Available online at www.sciencedirect.com
SCIENCE DIRECT
Journal of Catalysis 228 (2004) 43–55
JOURNAL OF CATALYSIS
www.elsevier.com/locate/jcat

Production of hydrogen from oxidative steam reforming of methanol I. Preparation and characterization of $Cu/ZnO/Al_2O_3$ catalysts from a hydrotalcite-like LDH precursor

M. Turco [a,*], G. Bagnasco [a], U. Costantino [b], F. Marmottini [b], T. Montanari [c], G. Ramis [c], G. Busca [c]

[a] *Dipartimento di Ingegneria Chimica, Università di Napoli Federico II, P.le V. Tecchio 80, 80125 Napoli, Italy*
[b] *CEMIN – Centro Eccellenza Materiali Innovativi Nanostrutturati, Dipartimento di Chimica, Università di Perugia, Via Elce di Sotto 8, 06123 Perugia, Italy*
[c] *Dipartimento di Ingegneria Chimica e di Processo "G.B. Bonino", Università di Genova, P.le J.F. Kennedy 1, 16129 Genova, Italy*

Received 10 May 2004; revised 2 August 2004; accepted 17 August 2004

Available online 25 September 2004

Abstract

Catalysts for oxidative methanol reforming were prepared by thermal and H_2-reduction treatments of a precursor consisting mainly of a hydrotalcite-like Cu–Zn–Al hydroxycarbonate and a Zn-rich paratacamite. The precursor was obtained by homogeneous precipitation of metal cations with a properly modified urea method. XRPD and quantitative Rietveld analysis of the precursor material revealed the presence of hydrotalcite and paratacamite phases in a weight ratio 3:1. Treatment in situ of the precursor produced $Cu/ZnO/Al_2O_3$ (Cu = 18%, Zn = 33%, Al = 49% mol) catalysts. Chemical properties of the precursor and of the catalysts were studied by TPR, TPO, NH_3-TPD, N_2O chemisorption, FTIR, and UV–vis techniques. Physical characterization was carried out by the SEM, EDS, XRPD, TG/DTA, and N_2 adsorption techniques. The influence of heating rate of the precursor was investigated. Heat-treated samples contained CuO, ZnO, and amorphous Al_2O_3, and probably $ZnAl_2O_4$, as suggested by XRPD and FTIR measurements. The crystallinity of oxide phases was higher for the sample treated with a lower heating rate that also showed lower surface area and lower Cu dispersion. The presence of Cu^{2+} in octahedral sites of alumina was suggested by UV–vis spectra. CO adsorption gave evidence of easy reduction of Cu(II) to Cu(I) and Cu(0) and the formation of stable complexes with Cu(I). NH_3-TPD and FTIR measurements showed the presence of surface acid sites of the Lewis type with wide strength distributions, mainly due to Zn^{2+} and Al^{3+} cations. Cu(II) was able to oxidize NH_3, while Cu(0) activated NH_3 decomposition. TPR and TPO measurements indicated that Cu species are easily reduced and reoxidized and Cu(I) species are intermediate for both processes. The redox properties appeared to be influenced by the rate of the previous heat treatment.
© 2004 Elsevier Inc. All rights reserved.

Keywords: Hydrotalcite; $Cu/ZnO/Al_2O_3$ catalysts; Methanol steam reforming; Rietveld analysis; IR characterization; Cu(I)–CO complexes; TPR/TPO characterization

1. Introduction

The technology of H_2-fed fuel cells, using polymeric electrolyte membranes (PEMFCs), is at present a promising alternative to internal combustion engines for car-traction due to their potentially very high efficiency [1]. On-board hydrogen production starting from a suitable liquid source appears to be a practical option in a medium-short perspective. Methanol may be preferable to other liquid hydrogen sources, such as gasoline, because it has high hydrogen content, can be reformed at relatively low temperatures (around 250 °C), and offers the advantages of the absence of sulfur compounds and less probable formation of carbonaceous products. Moreover, it could in theory be obtained from bio-

* Corresponding author. Fax: +39 081 5936936.
E-mail address: turco@unina.it (M. Turco).

0021-9517/$ – see front matter © 2004 Elsevier Inc. All rights reserved.
doi:10.1016/j.jcat.2004.08.026

masses like wood, and in this case the CO_2 produced should not contribute to the so-called greenhouse effect.

The oxidative steam reforming of methanol (OSRM) consists in the coupling of the endothermic methanol steam reforming (SRM) with the exothermic partial oxidation (POM) allowing the production of hydrogen with an autothermal process.

$$CH_3OH(g) + H_2O(g) = CO_2 + 3H_2, \quad \Delta H^0 = 49.5\ \text{kJ mol}^{-1}, \tag{1}$$

$$CH_3OH(g) + \frac{1}{2}O_2 = CO_2 + 2H_2, \quad \Delta H^0 = -192.3\ \text{kJ mol}^{-1}. \tag{2}$$

The OSRM catalysts proposed in the literature are closely related to those that have been deeply investigated for the synthesis of methanol [2–4]. They are mostly based on copper dispersed in a matrix formed by pure or mixed oxides like as ZnO [5–7], Al_2O_3 [8,9], ZnO/Al_2O_3 [10–13], Cr_2O_3/Al_2O_3 [8,14], and ZrO_2/Al_2O_3 [8]. These Cu-based catalysts have been studied previously for SRM [15–19] and POM [20–22]. Metallic copper is generally obtained by reduction of a Cu oxide phase that either is dispersed on a support such as Al_2O_3 or CeO_2 by impregnation [8,23] or is part of a mixed oxide system [6,7,12,13]. The best performances are obtained on catalysts containing also ZnO that acts as a promoter [8,10,18].

Promising OSRM catalysts can be obtained by heat treatment and reduction of mixed Cu, Zn, and Al hydroxycarbonates having hydrotalcite-like structures [12, 13,24,25]. These compounds, having the general formula $(Cu,Zn)_{1-x}Al_x(OH)_2(CO_3)_{x/2}\cdot mH_2O$, are generally prepared by coprecipitation with Na_2CO_3 solutions [24,26]. An alternative method, leading to materials with different textural properties, consists in precipitating the metal cations from a solution containing urea that is hydrolyzed to ammonium carbonate [12,27]. Thermal decomposition of such materials leads to an intimate mixture of oxides and the subsequent reduction with H_2 gives rise to highly dispersed metallic copper [12,13]. It is generally accepted that metallic Cu is the active phase in OSRM catalysts based on Cu/Zn/Al systems; however, oxidized Cu species are also present and their possible role in catalytic activity is greatly debated [7,11,12,24]. Redox properties of these systems are often studied by TPR and TPO techniques [12,28,29]. On the other hand acid–base properties have not been investigated, although they could play an important role in adsorption and activation of methanol [30,31]. Although characterization of these materials has been the object of several studies, it appears that some aspects need further investigation to obtain a deeper knowledge of the influence of the preparation procedure and the roles of the different catalysts phases on the OSRM reactions.

In this paper the preparation and the properties of a hydrotalcite precursor and of the derived $Cu/ZnO/Al_2O_3$ catalysts are described. The hydrotalcite precursor is obtained by coprecipitating Zn(II), Cu(II), and Al(III) cations with a modified urea method that allows a more precise control of the preparation conditions. Part I deals with the characterization by different complementary techniques of physical and chemical properties of the precursor and of the catalysts. The aim is to obtain information on the acid–base and redox properties of the catalysts that could be relevant in the OSRM catalysis. In Part II a study on catalytic activity and the reaction mechanism will be reported.

2. Experimental

2.1. Catalysts preparation

The catalyst precursor was obtained with the method of homogeneous precipitation accomplished by urea hydrolysis [27]. An aqueous solution, obtained by mixing 0.5 M $AlCl_3$, 0.5 M $ZnCl_2$, and 0.5 M $CuCl_2$ solutions in the volume ratio 1:1:1, was added of solid urea until the molar ratio urea/Al(III) was 6. The addition of the $CuCl_2$ solution has been carried out drop by drop, when the solution containing Zn and Al cations was at the boiling temperature. The solution was refluxed for 3 days. The precipitate obtained was separated from the mother solutions, washed with deionized water, and then suspended in a 0.05 M Na_2CO_3 solution (about 20 mL per gram of precipitate) for 1 day, in order to exchange chloride ions eventually present in the hydrotalcite material with carbonate anions. After equilibration with the Na_2CO_3 solution the solid was recovered, washed with deionized water, and finally dried at room temperature over P_4O_{10}. The catalysts were obtained by heating the precursor in dry air flow at rate of 2 or 10 °C min^{-1} up to 450 °C and maintaining it at this temperature for 12 h. Then the samples were reduced with H_2, according to procedures described in the following. The reducing treatments were effected in situ before characterization measurements.

The metal ion contents in the samples were obtained by ion chromatography, after dissolution in concentrated HCl. Determination of metal ion concentration in the obtained solution was performed with the following procedures: *Cu and Zn content*, column Dionex CS5a, eluent PDCA, flow 1.0 mL min^{-1}, spectrophotometric detection after PCR with PAR; *Al content*, column Dionex CS5a, eluent HCl 0.75 M, flow 1 mL min^{-1}, spectrophotometric detection after PCR with tiron.

The chloride content was determined by ion chromatography in the solution obtained by suspending the solid samples in 1 M Na_2CO_3 solution at 80 °C for 4 h. C, N, and H elemental analysis was obtained by a Carlo Erba 1106 analyzer. Carbonate and water contents were evaluated from thermogravimetrical analysis.

2.2. Catalyst characterization

X-ray powder diffraction (XRPD) patterns of the samples were recorded with a computer-controlled Philips PW1710

diffractometer using Cu-K_α Ni-filtered radiation (40 kV, 30 mA). XRPD patterns at programmed temperatures were taken in a HT A. Paar diffraction camera.

XRPD patterns used for quantitative Rietveld phase analysis were collected by means of a Bruker D8 Advance powder diffractometer, equipped with a θ–θ Bragg–Brentano geometry, using the Cu-K_α radiation and C/Ni Goebel-Spiegel mirror in the incident beam.

Scanning electron microscopy (SEM) and energy dispersion scanning (EDS) analyses were performed on both the precursor and the calcined materials by a Philips XL 30 instrument. TG analyses were performed in air by a Netzsch STA449C thermal analyzer at a heating rate of 5 °C min^{-1}.

N_2 adsorption–desorption isotherms were obtained at −196 °C, on samples previously degassed at 100 °C, using a computer-controlled Micromeritics 2010 apparatus. The application of the α_s-plot method [32] to adsorption data, using a nonporous CuZnAl-hydrotalcite as reference material, allowed us to evaluate the micropore volumes of the samples.

Copper areas were measured by the method of reaction with N_2O followed by TPR [33] using a Micromeritics 2900 apparatus. The sample, previously reduced at 450 °C in a 5% H_2/Ar mixture, was treated with pure N_2O at 60 °C for 1 h. TPR was carried out in a 5% H_2/Ar mixture at rate of 10 °C min^{-1}. The amount of chemisorbed O atoms was determined from the area of the TPR peak. Cu surface area and Cu dispersion were calculated assuming the stoichiometry O:Cu = 1:2 and concentration of Cu of 1.47×10^{19} atoms m^{-2} [33].

The IR spectra were recorded with a Nicolet Protégé 460 Fourier transform instrument. Infrared skeletal spectra of hydrotalcite precursor and of catalysts were obtained by the KBr pressed disk technique. The surface characterization was performed through in situ adsorption of suitable probe molecules: CO supplied by Air Liquide (adsorbed at RT or at −160 °C, 11 Torr pressure) and NH_3 (adsorbed at RT, 50 Torr pressure) supplied by Alphagaz. Pressed disks of pure catalyst powder (15 mg, 2 cm diameter) were used. The sample was thermally pretreated by outgassing at 450 °C in the IR cell. A conventional manipulation/outgassing ramp connected to the IR cell was used. The adsorption procedure involves contact of the activated sample disk with the gas of choice, and outgassing in steps from RT (or −160 °C) to higher temperatures. Spectra were collected after the thermal procedure and after each step of the adsorption procedure. In order to better evaluate the surface species from all the spectra herein reported the spectrum of the pretreated catalyst has been subtracted.

Diffuse reflectance spectra (DR-UV–vis-NIR) of pure sample powder (before and after calcination) were recorded by a Jasco V-570 apparatus in the range 50,000–4000 cm^{-1} at RT in air.

A Micromeritics 2900 apparatus equipped with a TCD detector was employed for TPR and TPO measurements. TPR measurements were carried out on calcined samples at a rate of 10 °C min^{-1} using a 5% H_2/Ar mixture. After the TPR test, the sample was cooled to room temperature in helium flow and then TPO measurement was carried out at a rate of 10 °C min^{-1} in 2% O_2/He flow.

NH_3 TPD measurements were carried out in a Micromeritics 2900 apparatus with TCD and MS detectors at a rate 10 °C min^{-1}, after the samples were saturated with pure NH_3 at RT.

3. Results and discussion

3.1. Catalyst preparation

The precursor of the OSRM catalysts was prepared with the urea method. This method allows the preparation of different hydrotalcite-like compounds containing Mg–Al, or Zn–Al, Ni–Al, and Mg–Fe having a high crystalline degree and a narrow particle-size distribution [27]. The presence of Cu^{2+} cations makes the synthetic procedure more complex, at least for two reasons. First, Cu^{2+} ions show the Jahn–Teller effect that favors the formation of distorted octahedral structures and preferentially gives rise to the precipitation of malachite phases. Secondarily, Cu^{2+} ions can be depleted by ammonia originated from urea hydrolysis. The preparation of Cu–Zn–Al precursors has required modification of the original urea method. In particular, the molar ratio urea/Al(III) has been decreased from 10 to 6 and addition of the $CuCl_2$ solution has been carried out drop by drop as described in Section 2. These modifications allowed us to obtain materials having a Cu content near, even if always lower, to that of the starting solution. However, most of the samples were polyphasic and pure hydrotalcite phases were obtained when the Cu content, expressed as molar ratio Cu^{2+}/total cations, was lower than 0.15. The effect of the different parameters influencing the urea method as well as of different preparation methods on the composition, phase analysis, and textural properties of hydrotalcite-like materials containing Cu cations will be published elsewhere. In the following the full chemical and physical characterization of a precursor obtained according to the procedure described in Section 2 and of the catalysts thereby obtained, that gave very good catalytic response, will be reported.

3.2. XRPD analysis

The XRPD pattern of the precursor is reported in Fig. 1. The pattern clearly indicates the good crystalline degree of the sample and the presence of two phases, identified as hydrotalcite (PDF N. 14-0191) and Zn-rich paratacamite (PDF N. 50-1558). Quantitative phase analysis was performed with the Rietveld method using the GSAS program, refining the scale factors and profile shapes for the two noted phases [34]. A small portion of the pattern (38.5–40° 2θ) was excluded from refinement because of the presence of a strong diffraction peak of the Al sample holder.

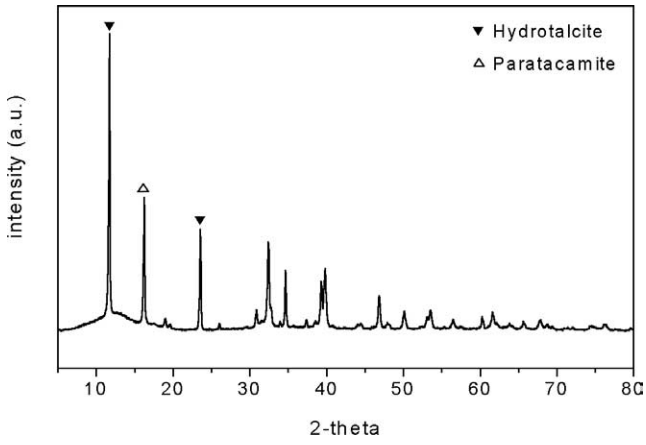

Fig. 1. XRPD pattern of hydrotalcite–paratacamite precursor conditioned over P_4O_{10}.

Table 1
Refinement details and quantitative phase analysis for the CuZnAl precursor

Angular range (°) 2θ	3–80
Step scan (°) 2θ	0.02
Time step (s)	15
R_p [a]	0.124
R_{wp} [b]	0.167
X [c]	5.15
Hydrotalcite (% w/w)	74.5 (2)
Paratacamite (% w/w)	25.5 (2)

[a] $R_p = \sum |I_o - I_c| / \sum I_o$.
[b] $R_{wp} = [\sum w(I_o - I_c)^2 / \sum w I_o^2]^{1/2}$.
[c] $\chi = [\sum w(I_o - I_c)^2 / (N_o - N_{var})]^{1/2}$.

The final Rietveld plot is shown in Fig. 2, while the refinement details are reported in Table 1. According to the phase analysis the sample consists of hydrotalcite and paratacamite in a weight ratio 3:1. The presence of a small amount of amorphous phases cannot be excluded. In comparison with similar Cu/Zn/Al hydrotalcite-like materials the present samples appear less complex regarding the phase composition. Materials obtained by coprecipitation with Na_2CO_3 [29] contained hydrotalcite, aurichalcite, and bayerite phases. In the following, notwithstanding the presence of a small amount of paratacamite, the precursor will be indicated as hydrotalcite precursor.

3.3. Elemental analysis and thermal behavior

Chemical analyses of the sample stored over P_4O_{10} gave the following results (expressed as mg g^{-1}): Zn^{2+} (210); Cu^{2+} (105); Al^{3+} (123); Cl^- (25); C (21); N (0); hydration water (50). The molar ratio of metals referred to total metals in the solid is thus 0.18, 0.33, and 0.49 for Cu, Zn, and Al, respectively. It may be noted that nitrogen compounds are not formed despite the presence of ammonia in the precipitating solution. The presence of chlorine can be assigned to the formation of Zn-rich paratacamite phase of formula $Cu_{2-x}Zn_x(OH)_3Cl$. Carbon content is assigned to carbonate present in the hydrotalcite phase. By assuming that only carbonates are the charge balancing anions, the Al content should be twice that of C content (1.75 mmol g^{-1}), that is, 3.50 mmol g^{-1}. By comparing this value with the total Al^{3+} content found (4.55 mmol g^{-1}), it can be deduced that 1.05 mmol g^{-1} of Al is present in the sample as amor-

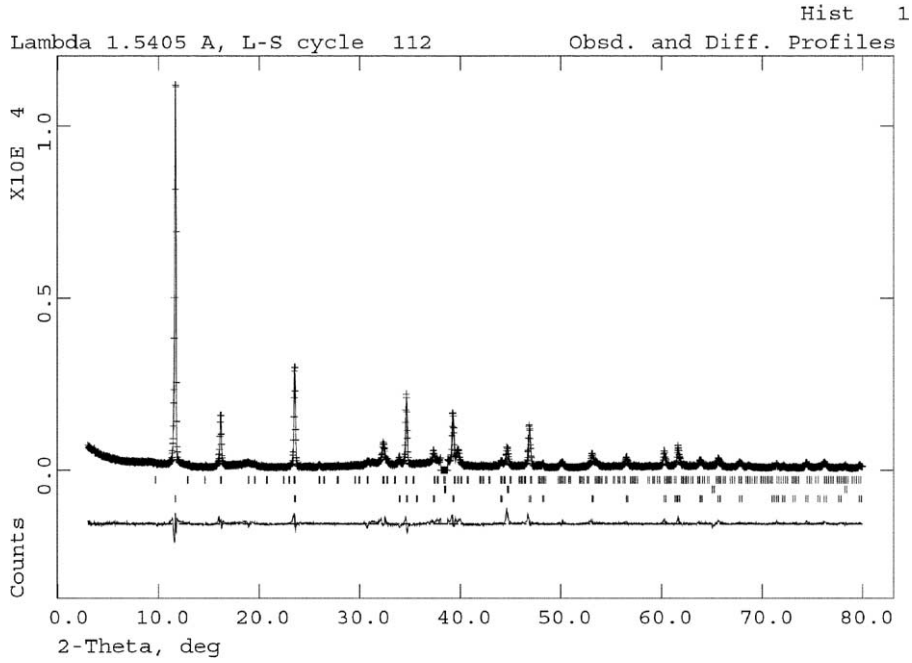

Fig. 2. Rietveld and difference plots for hydrotalcite and paratacamite phases present in the CuZnAl precursor. (Bottom lines: diffraction peak positions of hydrotalcite. Upper lines: diffraction peak positions of paratacamite.)

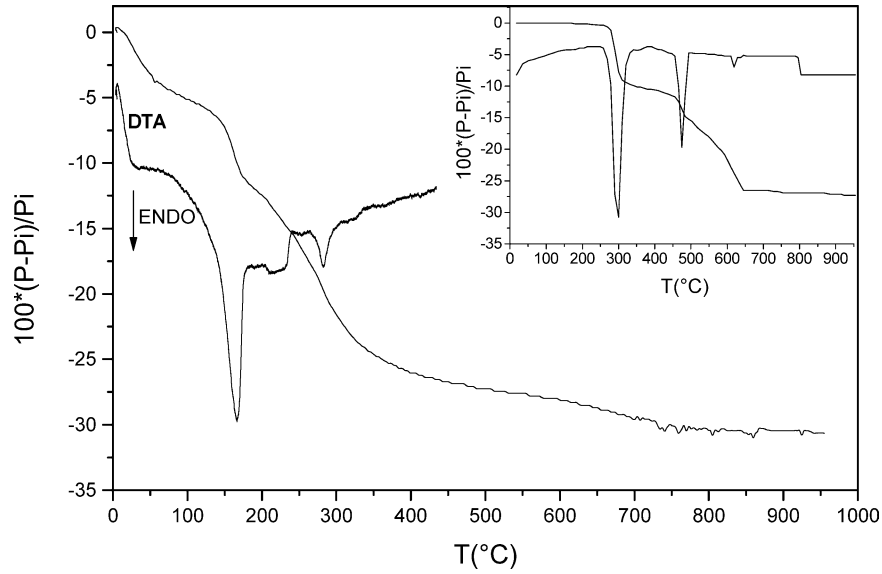

Fig. 3. TG/DTA curves of hydrotalcite precursor and (inset) paratacamite phase, previously conditioned over P_4O_{10}.

phous hydroxide. Since Cu^{2+} and Zn^{2+} are vicariant cations in both the hydrotalcite and the paratacamite phase it is difficult to assign an empirical formula to the two mixed phases. Fig. 3 shows the weight loss and differential thermal analysis curves of the precursor as a function of temperature. For sake of comparison, the inset of Fig. 3 reports the TG/DTA curves of a sample of paratacamite, prepared by the urea method. Thermal decomposition of paratacamite occurs in two well-differentiated steps. The first one, attributed to the loss of condensation water, is sharp and occurs at 300 °C, with a large endothermic effect. The second step, occurring between 450 and 650 °C, is broad with two endothermic effects and can be attributed to the loss of chlorine, very likely as HCl. At 700 °C only a mixture of Zn and Cu oxides is present. The TG/DTA curves of the precursor show the typical features of the thermal decomposition of hydrotalcite and paratacamite phases. The loss below 100 °C can be attributed to the loss of water cointercalated with carbonates in the hydrotalcite phase, while the loss over 450 °C to the decomposition of the paratacamite phase. The losses and the associated endothermic effects between 100 and 450 °C can be ascribed to the loss of condensation water of hydrotalcite (endothermic peak at 170 °C) and of paratacamite (peak at 300 °C) overlapping with the loss of carbonates. The total weight loss of the precursor (31%) is very near to that calculated for the thermal transformation of the precursor, having the composition reported above, into CuO, ZnO, and Al_2O_3 metal oxides.

The thermal decomposition of the precursor has been also monitored by recording the XRPD patterns in a HT diffraction camera. Fig. 4a shows the sequence of the patterns at increasing temperatures. It may be observed that the structure of the hydrotalcite phase (interlayer distance 7.51 Å) collapses at temperatures higher than 180 °C, while the characteristic peak of paratacamite (5.45 Å) is not present at temperatures higher than 260 °C, in agreement with the TG/DTA data. Over 320 °C, very weak reflections typical of the copper and zinc oxides start to appear. To have a better insight of the phases formed at temperatures higher than 400 °C, the XRPD patterns, taken at room temperature, of samples previously heated for 3 h in an oven at the indicated temperatures have been collected (see Fig. 4b). The patterns show diffraction peaks attributable to CuO and ZnO and only broad reflections attributable to zinc aluminate. Reflections of Al_2O_3 are absent. From these data, it appears that treatment at 450 °C is suitable for obtaining catalysts for OSRM. In fact, this temperature is sufficiently high for the formation of metal oxides, but low enough to avoid sintering phenomena that could cause loss of surface area. These samples, heated at 450 °C at two different heating rates (2 and 10 °C min^{-1}), hereafter indicated as 2-Cu/Zn/Al and 10-Cu/Zn/Al, have been used, after in situ H_2 reduction, as catalysts of the OSRM process. The different heating rate leads to samples having very similar XRPD patterns, but different specific surface areas and different redox properties (see later).

3.4. SEM and EDS analyses

SEM micrographs of the precursor and of the calcined material are reported in Figs. 5a and 5b. The precursor consists mainly of aggregates with dimensions of about 1–2 μm but some well-developed platelet-shaped crystals with dimension of about 7–8 μm are also detected. The particles of the sample treated at 450 °C maintain the same morphology of the original precursor, despite the dramatic change in composition. This effect, already observed in Mg–Al hydrotalcites [35], can be attributed to the so-called "memory effect" of hydrotalcites [36]. EDS analyses confirm the composition determined by chemical analysis, giving evidence

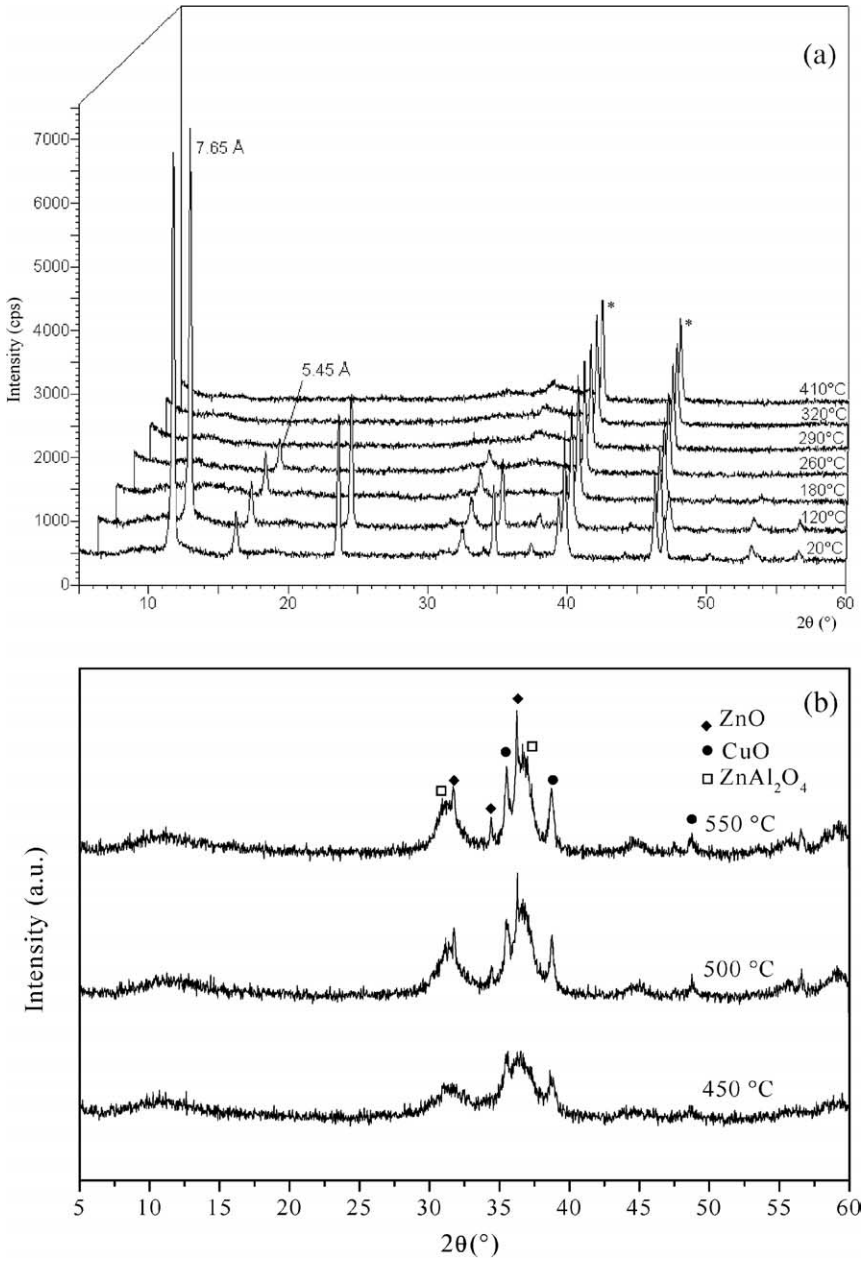

Fig. 4. XRPD patterns of hydrotalcite precursor: (a) sample heated in HT camera at the indicated temperatures, (b) samples heated for 3 h in oven at the indicated temperatures and then cooled at RT.

of uniform distribution of the elements throughout the samples.

3.5. Surface area and porosity

In Fig. 6 the N_2 adsorption isotherms of the precursor material and of samples treated at 450 °C with different heating rates are reported. All isotherms are of type II, according to the IUPAC classification. Calculated BET surface areas as well as micropore volumes, calculated by application of α_s-plot method to adsorption data, are reported in Table 2.

As expected, thermal treatment at 450 °C causes a decrease of the specific BET surface areas that, however, are still high. The decrease is modest (from 133 to 111 $m^2\,g^{-1}$) when the precursor is heated at a higher heating rate, 10 °C min^{-1}, much more consistent (from 133 to 73 $m^2\,g^{-1}$) at a lower heating rate, 2 °C min^{-1}. For all the samples, negligible mesopore volume is found, while a small micropore volume is measured. It is worth noting that the different heating rates produce samples with different specific surface areas and pore volumes even if the XRPD patterns and SEM analysis do not show remarkable differences.

The Cu surface areas and Cu dispersions of the reduced samples, measured by the method of N_2O chemisorption,

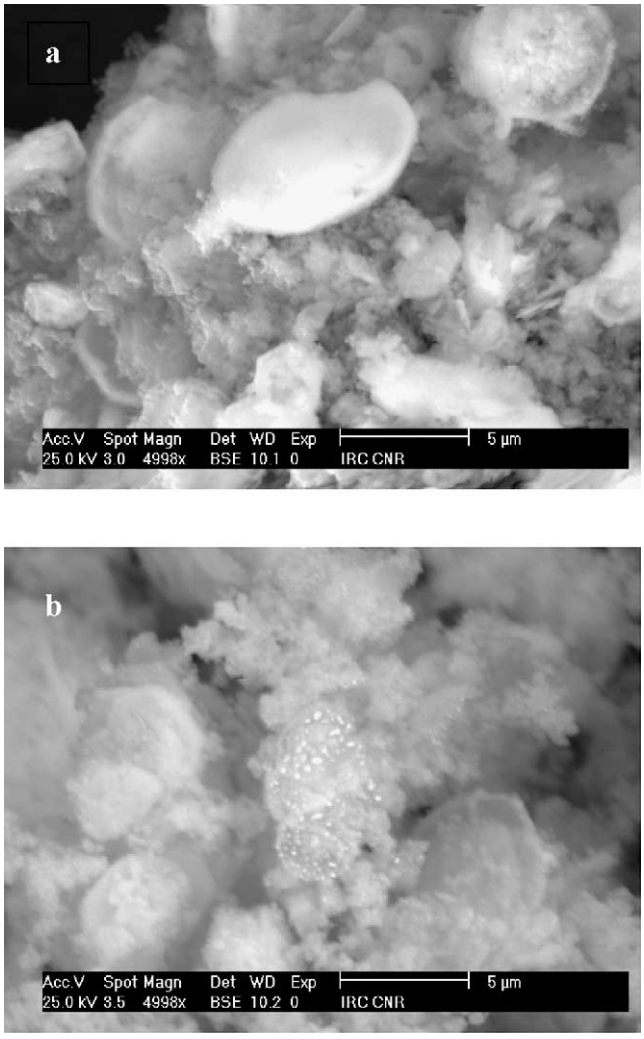

Fig. 5. SEM micrographs of: (a) hydrotalcite precursor; (b) 10-Cu/Zn/Al sample.

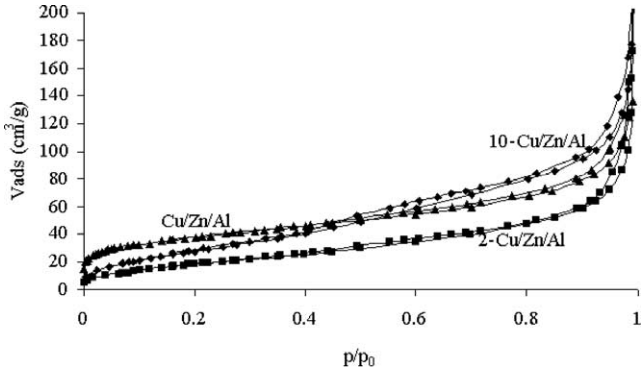

Fig. 6. N_2 adsorption isotherms of hydrotalcite precursor and 2-Cu/Zn/Al and 10-Cu/Zn/Al samples.

are reported in the same Table 2. Such reduced samples correspond to ready-to-use catalysts as employed in Part II of this paper. It can be noted that Cu dispersion is slightly affected by the rate of the previous heat treatment: probably the higher heating rate leads to a more disperse CuO phase that favors the dispersion of the derived Cu phase.

Table 2
Surface area and pore volume of precursor and calcined samples; Cu surface area and Cu dispersion of reduced samples

Sample	Specific surface area ($m^2\ g^{-1}$)	Micropore volume ($cm^3\ g^{-1}$)	Cu surface area ($m^2\ g^{-1}$)	Cu dispersion (%)
Precursor	133	0.055	–	–
2-Cu/Zn/Al	73	0.021	9.2	8.3
10-Cu/Zn/Al	111	0.056	10.1	9.1

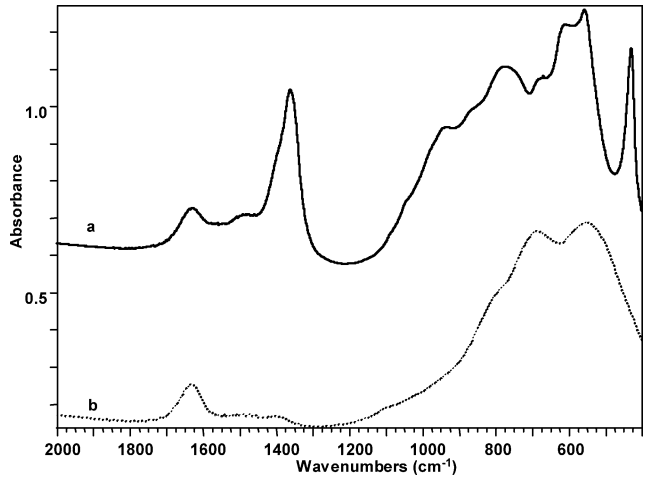

Fig. 7. FTIR spectra of (a) hydrotalcite precursor and (b) calcined 10-Cu/Zn/Al catalyst recorded in air at RT using the KBr method.

3.6. *Infrared study of the hydrotalcite precursor and of its thermal decomposition*

The infrared spectrum of the precursor material (Fig. 7a) in the spectral range 2000–400 cm^{-1} is quite complex, showing bands around 431, 558, 616, 682, 772, 865, 945, and 1044 cm^{-1}. The bands are relatively sharp indicating, according to XRPD patterns (see Fig. 1), a high degree of crystallinity. The spectrum fully agrees with the published spectra of hydrotalcite-like double hydroxides [37,38]. Controversy exists about the assignation of the bands. However, by comparison with the data reported by Kloprogge and Frost [37] for Mg–Zn–Al hydrotalcites, we can give the following assignments: 431 cm^{-1}, Zn–OH deformation, otherwise $[AlO_6]^{3-}$ or a single Al–O bond; 558 and 616 cm^{-1}, Al/Cu–OH translations, 772 cm^{-1}, Al–OH translation; 865 cm^{-1}, interlayer CO_3^{2-} deformation; 945 cm^{-1}, Al/Zn–OH deformation: 1044 cm^{-1}, Al–OH deformation.

Additional components due to carbonate species are found at higher frequencies: two well-defined bands are located at 1362 and 1483 cm^{-1}. The further band at 1630 cm^{-1} is due to H–O–H deformation of water molecules.

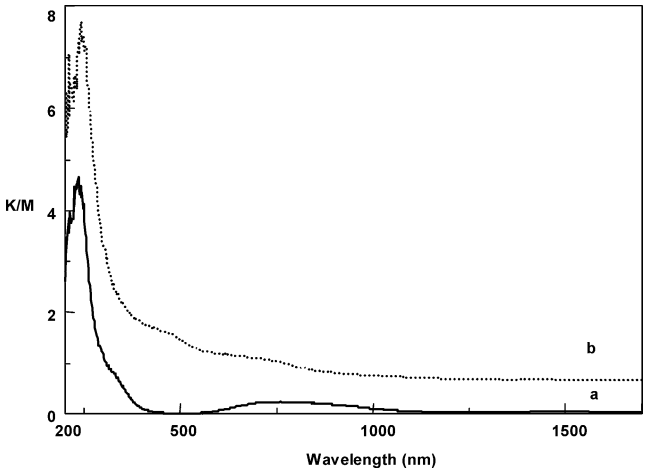

Fig. 8. DRS-UV–vis spectra of (a) hydrotalcite precursor and (b) calcined 10-Cu/Zn/Al catalyst recorded in air at RT.

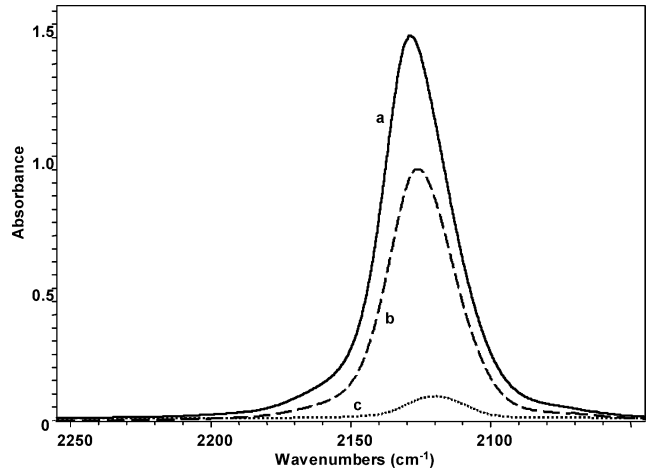

Fig. 9. Adsorption of CO at RT over the 10-Cu/Zn/Al catalyst pretreated under vacuum at 200 °C. Surface species (a) after contact with the gas, (b) after 1 min outgassing at RT, (c) after 10 min outgassing at RT. The spectrum of the catalyst after thermal pretreatment was subtracted.

After calcination at 450 °C (sample 10-Cu/Zn/Al; Fig. 7b) the spectrum shows a significant change: it is now dominated by a broad complex absorption with two main maxima near 570 and 700 cm^{-1} and with well evident shoulders near 800 and 1100 cm^{-1}. The bands of carbonate species almost completely disappeared, and those due to the metal–oxygen stretching of the original hydrotalcite structure are absent. According to XRPD patterns, these data indicate the formation of a mixed oxide system. The IR features observed with the calcined sample are typical of the spinel structure and can be related mainly to the formation of γ-Al_2O_3 and of $ZnAl_2O_4$. So, the two main absorption bands at 700 and 570 cm^{-1} can be assigned to the so-called ν_1 and ν_2 vibrational mode of isolated [AlO_4] or [ZnO_4] tetrahedra and [AlO_6] octahedra, respectively [39].

3.7. UV–vis spectra

The UV–vis spectra of the precursor and the calcined material (10-Cu/Zn/Al) are reported in Fig. 8. The precursor shows a very broad and weak band around 800 nm that can be assigned to d–d transitions of Cu^{2+} ions in a distorted octahedral symmetry [13]. The band at 330 nm is probably due to charge transfer transitions involving Cu^{2+}–O^{2-}–Cu^{2+} species [13,40]. The strong band around 240 nm can be attributed to $O^{2-} \rightarrow Cu^{2+}$ ligand to metal charge transfer transition [13].

The spectrum of the calcined sample presents a stronger band around 240 nm and a broad one around 710 nm; according to previously reported data [13], these two features are typical of copper oxide–alumina samples. The band at 710 nm in particular has been assigned to the $^2E_g \rightarrow {}^2T_{2g}$ spin-allowed d–d transition of Cu^{2+} ions in the distorted octahedral environment of the surface alumina sites with a spinel-type structure. The absorption around 400 nm could be due to ZnO segregated after calcination.

3.8. FTIR study of adsorption of carbon monoxide on the catalyst

Adsorption of CO (IR band of the gas at 2138 cm^{-1}) is one of the most useful methods for characterizing the nature of dispersed transition metal species over catalytic surfaces [41]. Moreover, CO adsorption in this case can be particularly relevant because it is an unwanted product and/or a key intermediate of the overall OSRM reaction and it plays an important role in the reaction under study.

Adsorption of CO at RT over 10-Cu/Zn/Al catalyst pretreated under vacuum at 200 °C (Fig. 9a) leads to the appearance of a complex band with the maximum centered at 2130 cm^{-1} and a weak shoulder on its higher frequency side, near 2165 cm^{-1}. Outgassing at RT causes a strong decrease of the intensity and a shift of the main maximum down to 2120 cm^{-1}, while the shoulder at higher frequency is completely eroded (Figs. 9b and 9c).

After contact of the catalyst surface with CO at −160 °C (Fig. 10a), bands at 2135 (probably a multiple band), 2167, and 2189 cm^{-1} are detected. By increasing the contact time (Figs. 10b and 10c), the spectra show significant changes: (i) the band at a lower frequency slightly increases in intensity and shifts to 2140 cm^{-1}, while a new component at lower frequency seems to appear; (ii) the intensity of 2189 and 2167 cm^{-1} bands strongly increases, the latter becoming the most intense after 10 min. Only a weak band at 2135 cm^{-1} with shoulder at lower frequency resists evacuation at RT (Fig. 10d).

Adsorption of CO at −160 °C on the catalyst activated at a higher temperature (300 °C) gives rise to a complex band characterized by a maximum at 2128 cm^{-1} with a shoulder at 2135 cm^{-1} and two weaker bands at 2163 and 2187 cm^{-1} (Fig. 11a). Outgassing at the same temperature (Fig. 11b) causes a significant decrease in intensity of the bands at 2187 and 2163 cm^{-1}, and the disappearance of the lower fre-

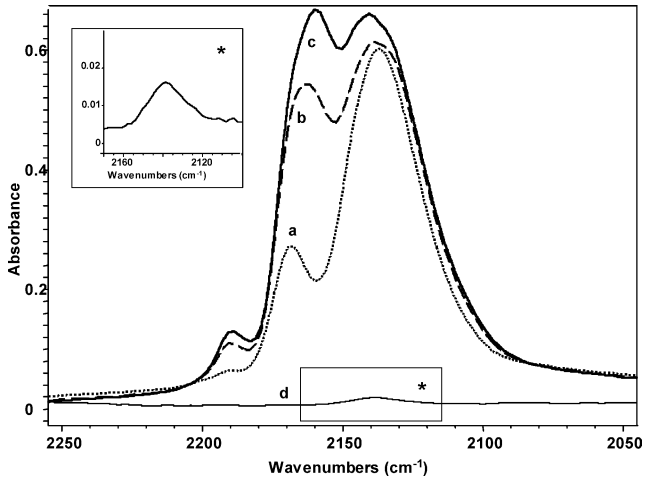

Fig. 10. Adsorption of CO at −160 °C over the 10-Cu/Zn/Al catalyst pretreated under vacuum at 200 °C. Surface species at increasing contact time with the gas: (a) after 0 min, (b) after 5 min, (c) after 10 min. Surface species after evacuation at RT (d). The spectrum of the catalyst after thermal pretreatment was subtracted.

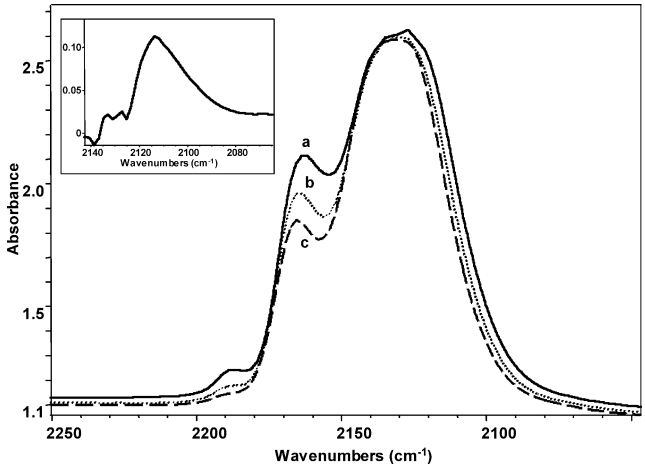

Fig. 11. Adsorption of CO at −160 °C over the 10-Cu/Zn/Al catalyst pretreated under vacuum at 300 °C. Surface species (a) after contact with the gas, (b) after evacuation at −160 °C, (c) after evacuation at −140 °C. The spectrum of the catalyst after thermal pretreatment was subtracted. Inset: (c)–(a) subtraction spectrum.

quency component of the main band, while the component at 2135 cm^{-1} seems practically unperturbed. After outgassing on warming up to −140 °C (Fig. 11c), a further decrease in intensity of the bands at 2187 and 2163 cm^{-1} takes place, while the band at 2135 cm^{-1} appears still unaltered.

According to previous work [42–45] the band observed after CO adsorption at low temperature at 2135 cm^{-1} (Fig. 10a) and at 2130–2120 cm^{-1} after CO adsorption at room temperature, quite stable to outgassing, can be confidently assigned to the Cu^{+}–CO species. It is in fact well known that stable carbonyls are formed over monovalent copper cations, responsible for a νCO band a little below the gas-phase value. In fact, the quite strong σ-type donation of the C lone pair of CO is reinforced by a relevant π-type back bonding from the d orbitals of cuprous ion to the antibonding orbitals of CO. The formation of Cu(I) species was already observed in Cu/Zn/Al catalysts subjected to reducing treatments or used in the OSRM process by the XPS technique [11,24].

The band near 2160 cm^{-1}, i.e., well above the gas-phase νCO value, very intense over the surface of the catalyst activated at 200 °C (Fig. 10a), and less intense over the surface of the catalyst activated at 300 °C (Fig. 11a), can be confidently assigned to CO adsorbed over Cu^{2+} species. This band is much weaker at room temperature because of the instability of the Cu^{2+}–CO carbonyls, due in part to the weakness of the coordination bond (where back bonding is poor or nothing) and in part to the ability of Cu^{2+} in oxidizing CO to CO_2 (or carbonate species).

Finally the presence of carbonyl species over metallic copper surface sites can be deduced from the presence of a component at 2128 cm^{-1} detected after adsorption at low temperatures over the catalyst pretreated at 300 °C, that quickly disappears even after evacuation at −140 °C (Fig. 11c). This component is well evident in the subtraction spectrum reported as an inset in Fig. 11. Both CO frequency and thermal behavior fully agree with those typical of carbonyls over Cu metal particles.

The further weak band observed around 2190 cm^{-1} (Figs. 10 and 11) is assigned to CO coordinated to the mixed oxide support. These data show how easy the redox cycles are for Cu species that are reduced to Cu^{+} and Cu^{0} too by simple outgassing as well as by the reducing agents present in the atmosphere.

3.9. FTIR study of adsorption of ammonia on the catalyst

In order to gain information about the acid–base properties of the catalyst, which could be relevant with respect to methanol and water adsorption, we investigated the adsorption of ammonia by FTIR spectroscopy. In Fig. 12a the spectrum of the adsorbed species arising from ammonia adsorption at RT on the catalyst preactivated by outgassing at 450 °C is reported. It shows two strong bands, both quite broad, with the main maxima at 1614 and 1244 cm^{-1}, respectively. Other weak absorptions are observable at 1449 cm^{-1}, and in the region 2200–2000 cm^{-1}. The strongest band with the main maximum at 1244 cm^{-1}, but with a tail toward its lower frequency side, is due to the symmetric deformation of coordinated ammonia, $\delta_{sym}NH_3$. The higher frequency band is the corresponding asymmetric deformation mode, $\delta_{as}NH_3$. As expected indeed, no bands due to ammonium ion are observed, showing the absence of Brønsted acidity on the catalyst surface.

According to the sensitivity of the position of the $\delta_{sym}NH_3$ mode to the Lewis acid strength of the adsorbing cation, the IR data give evidence of the presence of cationic sites characterized by a medium-strong Lewis acidity, as predominant adsorbing sites. The width and position of this band are similar to those observed previously, e.g., over Mg–Al

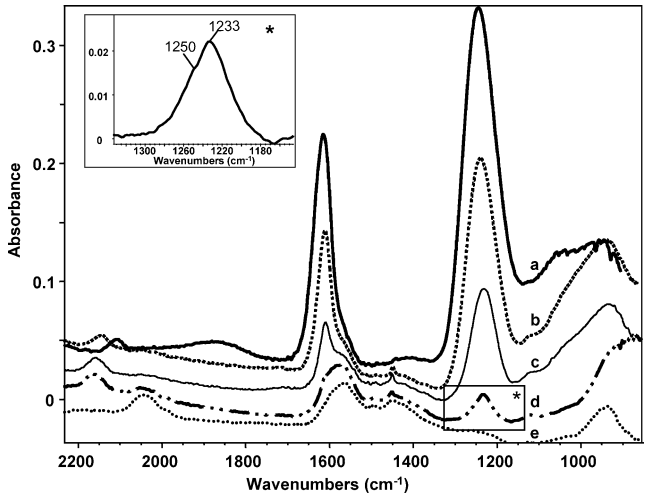

Fig. 12. Adsorption of NH_3 at RT over the 10-Cu/Zn/Al catalyst pretreated under vacuum at 450 °C. Surface species (a) after contact with the gas, (b) after evacuation at RT, (c) after evacuation at 100 °C, (d) after evacuation at 200 °C, (e) after evacuation at 300 °C. The spectrum of the catalyst after thermal pretreatment was subtracted.

and Cu–Mg–Al mixed oxides produced by decomposition of hydrotalcite-like precursors [46].

Evacuation at RT (Fig. 12b) causes a relevant decrease of the intensity of these bands. After outgassing at increasing temperature (Figs. 12c–12e) the bands due to coordinated ammonia decrease even more, as expected, and the symmetric deformation mode, $\delta_{sym}NH_3$, now shows the maximum at 1233 with a shoulder at 1250 cm^{-1} (Fig. 12) which could be assigned to ammonia coordinated over Zn^{2+} and Al^{3+} ions, respectively.

The weak sharp band at 1449 cm^{-1} has already been detected by us after ammonia adsorption over Cu-based catalysts and other transition metal oxide catalysts [44,47,48] and has been assigned to species produced by ammonia oxidation and likely intermediates in the formation of hydrazine, the likely precursor of N_2. Also the bands in the region 2200–2000 cm^{-1} have been detected frequently [49] and are certainly due to N–O bond stretchings of ammonia oxidation species.

Therefore these results clearly show that Lewis acid sites with medium-high strength, mostly due to the Zn–Al oxide "support," are present on the surface of the catalyst. A fraction of the adsorption sites, probably involving oxidized Cu centers, show noticeable oxidative properties, as suggested by the formation of ammonia oxidation products; so this shows their quite easy reducibility.

3.10. TPR/TPO measurements

The TPR profiles of 2-Cu/Zn/Al and 10-Cu/Zn/Al are reported in Fig. 13. The TPR curve of pure CuO is also reported for comparison. The TPR profile of pure CuO shows a single peak with maximum at 342 °C. The Cu/Zn/Al materials give composite peaks, with two not resolved signals in the same temperature range as pure CuO. The two peaks,

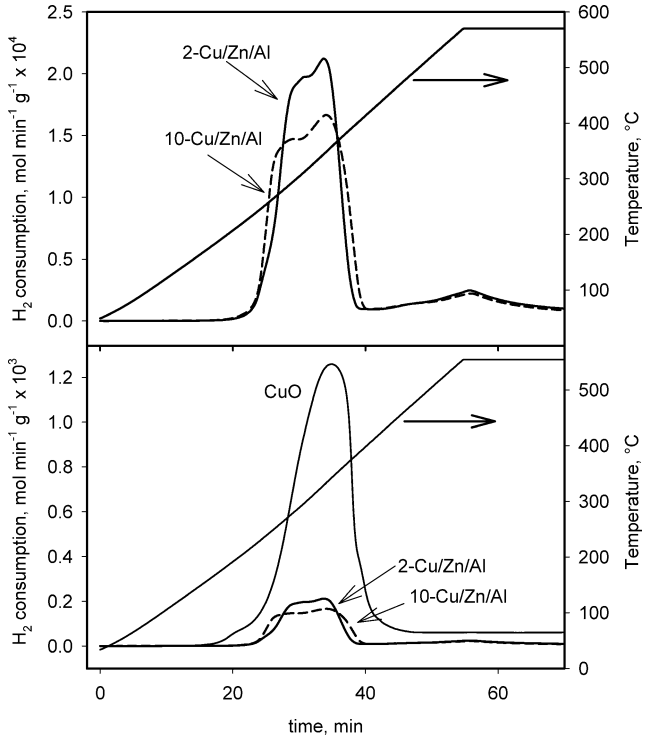

Fig. 13. TPR profiles of 2-Cu/Zn/Al and 10-Cu/Zn/Al samples and CuO.

Table 3
Results of TPR measurements

Sample	T_{max} (°C)	H_2 consumption	
		mol g^{-1}	mol mol^{-1}_{Cu}
CuO	342	1.25×10^{-2}	1.00
2-Cu/Zn/Al	310, 344	1.98×10^{-3}	0.97
10-Cu/Zn/Al	290, 345	2.05×10^{-3}	1.00

with maxima at about 290–310 and 345 °C, appear of similar intensity, although the single components cannot be exactly resolved. The TPR profile of the sample 2-Cu/Zn/Al appears sharper; however, the amount of consumed hydrogen, reported in Table 3, is the same for the two materials and corresponds to reduction of all Cu(II) to Cu(0). Composite TPR peaks were also reported by other authors for Cu/Zn/Al systems, either with high [12] or with low alumina content [13]. Different TPR components were explained by reduction of different Cu(II) species, such as CuO, $CuAl_2O_4$, and Cu^{2+} ions incorporated in octahedral sites of the Al_2O_3 phase [12,13]. In our samples, besides the CuO phase detected by XRPD, some Cu^{2+} ions are probably present in the surface sites of alumina and the two TPR signals could be related to reduction of different Cu(II) species. However, it is expected that the limited amount of surface Cu(II) species contribute to TPR signals to a lower extent than bulk CuO. Therefore, it seems more likely that the two TPR components are related to the two-step reduction: Cu(II) → Cu(I) → Cu(0), as suggested by [8]. A two-step reduction of Cu(II) was also observed for CuO/ZnO catalysts by the XANES technique [7,18], although in this case the two signals were not dis-

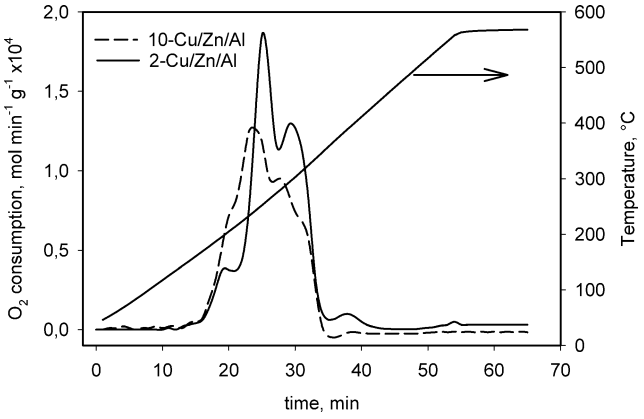

Fig. 14. TPO profiles of 2-Cu/Zn/Al and 10-Cu/Zn/Al samples.

tinguished by the TPR technique. From data by different authors [8,15,28,50] it seems that the two reduction steps of Cu(II) are not distinguishable by the TPR technique when Cu(II) species are highly concentrated. This could be due to (i) a broadening of the peaks in the presence of high amount of Cu(II), or (ii) the large heat release that increases the temperature of the sample speeding up the second reduction step. Some authors found that highly dispersed CuO gave TPR signals at much lower temperatures than bulk CuO [15,50,51]; since such signals are absent in our TPR spectra, we can exclude the presence of a highly dispersed form of CuO. According to the XRPD and UV–vis analyses our samples contain, besides CuO, Cu(II) species as vicariant species in the zinc oxide and zinc aluminate: these species should be reduced at a temperature higher than that of CuO [13] and could be related to the small signal that appears at about 570 °C in TPR profiles. However, on the whole the TPR profiles of these samples show less components than similar hydrotalcite-derived Cu/Zn/Al catalysts [29] and this is probably related to a more homogeneous phase composition. The different shape of TPR profiles of the two samples could be related to the different specific surface area: the sample 10-Cu/Zn/Al, obtained with a higher heating rate has a higher surface area and very likely is less homogeneous (as regards crystals sizes), thus showing a wider range of reduction temperature. This agrees with the higher dispersion of the Cu phase in the sample 10-Cu/Zn/Al, as above discussed.

In order to obtain more complete information on redox properties, TPO measurements were effected on the samples after TPR tests, thus containing metallic Cu. In Fig. 14 we report TPO curves of 2-Cu/Zn/Al and 10-Cu/Zn/Al. The two samples show composite TPO peaks in which two main components are well evident at about 240–250 and 300 °C and a shoulder is also present at about 200 °C. The amounts of consumed oxygen (Table 4) are close to that corresponding to oxidation of all Cu(0) to Cu(II). The two main TPO signals can be related to the two oxidation steps Cu(0) → Cu(I) → Cu(II). The formation of Cu(I) as intermediate species during oxidation of Cu(0) at 250 °C was already observed in similar materials [18].

Table 4
Results of TPO measurements

Sample	T_{max} (°C)	O_2 consumption	
		mol g^{-1}	mol mol_{Cu}^{-1}
2-Cu/Zn/Al	203 (sh), 254, 300	1.41×10^{-3}	0.67
10-Cu/Zn/Al	200 (sh), 245, 282	1.38×10^{-3}	0.63

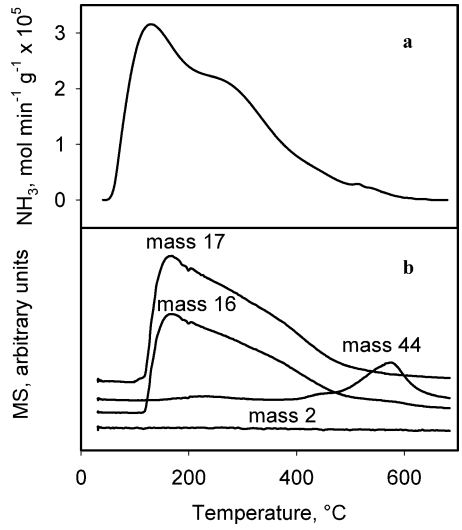

Fig. 15. NH_3 TPD spectra of oxidized 10-Cu/Zn/Al sample: (a) TCD detector; (b) MS detector.

It is worth noting that the sample 10-Cu/Zn/Al shows broader and less resolved signals with a more intense low-temperature shoulder. This means that the properties of the Cu phase are appreciably influenced by the previous heating rate. As observed above, the CuO phase contained in the sample 10-Cu/Zn/Al is more heterogeneous: this could lead, after reduction, to a more heterogeneous Cu phase, with a wider distribution of particle sizes. This effect can explain the presence of broader TPO signals, due to different oxidation rate of particles of different sizes.

The component that appears as a shoulder at about 200 °C could be due to a surface oxidation that is kinetically faster and precedes the bulk oxidation. This component is more intense for the sample 10-Cu/Zn/Al, suggesting the presence of particles with lower average dimensions, as expected for the sample obtained with higher heating rates.

3.11. NH_3-TPD measurements

NH_3 TPD measurements were carried out both on calcined samples and on samples reduced according to the TPR conditions. NH_3 thermodesorption was monitored by TCD and MS detectors. In Figs. 15 and 16 the corresponding curves are reported.

TPD spectrum of not-reduced 10-Cu/Zn/Al sample (Fig. 15a) shows a composite signal due to at least two components, with maximum at 129 °C and a broad shoulder at about 350 °C and a long tail extending up to 600 °C.

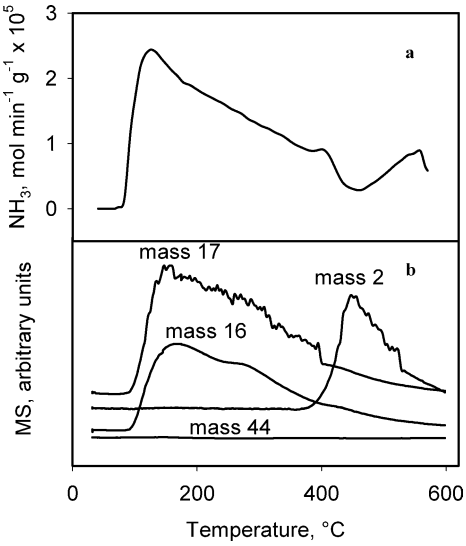

Fig. 16. NH_3 TPD spectra of reduced 10-Cu/Zn/Al sample: (a) TCD detector; (b) MS detector.

This is indicative of a wide strength distribution of acid sites, varying from weak to strong. These acid sites are related to the contribution of the different metal oxides Al_2O_3, ZnO, CuO, although the contribution of Al_2O_3 is probably prevailing. The amount of desorbed ammonia is 8.8×10^{-4} mol g^{-1} corresponding to surface site concentration of 4.7×10^{14} cm^{-2}. In agreement with the above IR study, ammonia is adsorbed on Lewis acid sites, identified above predominantly as Zn^{2+} and Al^{3+} cations. In the MS spectra (Fig. 15b) the signals of mass 16 and 17 that are due to ammonia closely correspond to the TCD signal, showing that NH_3 is mainly desorbed as unreacted species. The absence of peaks of mass 28 and 2 gives evidence that ammonia undergoes no decomposition during thermodesorption. However, a well evident peak with maximum at 580 °C appears in the spectrum of mass 44 corresponding to N_2O species. This peak appears in correspondence of the tail of the ammonia signal and so is related to interaction of NH_3 with strong and oxidizing adsorbing sites, which are certainly associated with Cu^{2+} cations, in agreement with FTIR measurements.

On the sample reduced as described above a TPD measurement was performed and the results are reported in Fig. 16. A composite peak is observed also under this condition (Fig. 16a), with a shape resembling that of the not-reduced sample in the low-temperature range, while a swinging signal is observed in the temperature range 400–600 °C. The amount of desorbed ammonia is similar to that observed for the not-reduced sample (7.6×10^{-4} mol g^{-1}, corresponding to surface sites concentration of 4.1×10^{14} cm^{-2}). MS spectra of mass 16 and 17 (Fig. 16b) show no swinging of the signal and are very similar to those of the not-reduced sample, showing shouldered peaks with maxima at about 150 °C and a long tail extending up to 600 °C. This indicates that the reduced sample also shows a wide distribution of acid strength, from weak to strong, and acidic properties are not influenced by H_2 reduction because they are related to the metal oxide matrix in which the Cu(0) phase is dispersed. The MS spectra indicates that NH_3 is desorbed mainly as unreacted species since no signals of mass 44 are observed (Fig. 16b). This suggests that no oxidation of ammonia occurs in the entire temperature range, different from the not-reduced sample. On the other hand, a well evident peak of mass 2 appears in the same temperature range where the peak of mass 44 appeared with the not-reduced sample. The presence of hydrogen explains the swinging of the TCD signal at high temperatures, since H_2 can give negative signals with TCD when He is employed as carrier gas. The formation of H_2 can be due to some decomposition of ammonia catalyzed by Cu(0). Therefore these results indicate catalytic dehydrogenating properties of metallic copper formed by reduction of Cu(II).

The results of NH_3 TPD measurements can be summarized as follows:

- the calcined sample has acid sites with a wide strength distribution, from weak to strong; such acid strength distribution is retained after reduction with H_2;
- Cu(II) species behave as strong adsorbing sites characterized by noticeable oxidant properties;
- the metallic copper, formed by reduction of the sample, exhibits dehydrogenating properties.

4. Conclusions

This study has dealt with the synthesis and characterization of complex materials in light of their use as catalysts for methanol reforming. It may be anticipated (see Part II of the work) that the catalysts obtained have shown very interesting catalytic performance and this accounts for the efforts made in their wide characterization. In particular, a Cu/Zn/Al hydrotalcite-like material has been prepared with the urea method, modified to introduce Cu(II) into the brucite sheets. This has allowed us to obtain a product with fairly high Cu content; however, the contemporary formation of a Cu/Zn oxychloride (paratacamite phase) could not be avoided. In comparison with literature data, precursors prepared by the urea hydrolysis method appear more homogeneous and lead to catalysts with different redox properties.

In this work the thermal behavior of the precursor has been thoroughly investigated, and formation of a very dispersed mixed oxide system has been observed above 320 °C. Spectroscopic measurements have shown that, after treatment at 450 °C, besides CuO, ZnO, and amorphous Al_2O_3, also Cu and Zn aluminates are probably present.

Acid and redox properties of calcined samples, that can play an important role in the catalysis of OSRM reactions, have been characterized. The presence of Brønsted acidity has been excluded, while Lewis acid sites with a wide strength distribution have been detected.

Noticeable oxidizing properties of Cu(II) centers have been evidenced, while metallic copper has been shown to possess catalytic dehydrogenating properties. It has been hypothesized that reduction of CuO and reoxidation of Cu(0) occurs through the formation of Cu(I) intermediate species. Cu(I) species are able to form stable complexes with CO molecules, while Cu(0) and Cu(II) interact very weakly with CO. Also this property could play an important role in the mechanisms of the OSRM reactions.

Acknowledgments

This research was founded by Ministero Istruzione Università e Ricerca and Genova, Napoli, and Perugia Universities in the framework of Programmi di Ricerca di Interesse Nazionale, 2002 No. 038793. The authors acknowledge Mr. Luciano Cortese for contribution to TPR/TPO and NH_3 TPD measurements.

References

[1] R.F. Service, Science 285 (1999) 682.
[2] K. Klier, Adv. Catal. 31 (1982) 243.
[3] K.C. Waugh, Catal. Today 15 (1992) 51.
[4] G. Busca, M.E. Pattuelli, F. Trifirò, A. Vaccari, Stud. Surf. Sci. Catal. 48 (1989) 239.
[5] F. Raimondi, B. Schnyder, R. Kotz, R. Schelldorfer, T. Jung, J. Wambach, A. Wokaun, Surf. Sci. 532–535 (2003) 383.
[6] T.L. Reitz, S. Ahmed, M. Krumpelt, R. Kumar, H.H. Kung, J. Mol. Catal. A: Chem. 162 (2000) 275.
[7] T.L. Reitz, P.L. Lee, K.F. Czaplewski, J.C. Lang, K.E. Popp, H.H. Kung, J. Catal. 199 (2001) 193.
[8] B. Lindström, L.J. Pettersson, P.G. Menon, Appl. Catal. A 234 (2002) 111.
[9] P. Mizsey, E. Newson, T. Truong, P. Hottinger, Appl. Catal. A 213 (2001) 233.
[10] K. Geissler, E. Newson, F. Vogel, T.B. Truong, P. Hottinger, A. Wokaun, Phys. Chem. Chem. Phys. 3 (2001) 289.
[11] F. Raimondi, K. Geissler, J. Wambach, A. Wokaun, Appl. Surf. Sci. 189 (2002) 59.
[12] S. Murcia-Mascarós, R.M. Navarro, L. Gómez-Sainero, U. Costantino, M. Nocchetti, J.L.G. Fierro, J. Catal. 198 (2001) 338.
[13] S. Velu, K. Suzuki, M. Okazaki, M.P. Kapoor, T. Osaki, F. Ohashi, J. Catal. 194 (2000) 373.
[14] B. Lindström, J. Agrell, L.J. Pettersson, Chem. Eng. J. 93 (2003) 91.
[15] J.P. Breen, J.R.H. Ross, Catal. Today 51 (1999) 521.
[16] B.A. Peppley, J.C. Amphlett, L.M. Kearns, R.F. Mann, Appl. Catal. A 179 (1999) 21.
[17] B.A. Peppley, J.C. Amphlett, L.M. Kearns, R.F. Mann, Appl. Catal. A 179 (1999) 31.
[18] M.M. Günter, T. Ressler, R.E. Jentoft, B. Bems, J. Catal. 203 (2001) 133.
[19] N. Takezawa, N. Iwasa, Catal. Today 36 (1997) 45.
[20] L. Alejo, R. Lago, M.A. Peña, J.L.G. Fierro, Appl. Catal. A 162 (1997) 281.
[21] R.M. Navarro, M.A. Peña, J.L.G. Fierro, J. Catal. 212 (2002) 112.
[22] Z. Wang, W. Wang, G. Lu, Int. J. Hydrogen Energy 28 (2002) 151.
[23] W.-H. Cheng, I. Chen, J. Liou, S.-S. Lin, Top. Catal. 22 (2003) 225.
[24] S. Velu, K. Suzuki, C.S. Gopinath, J. Phys. Chem. B 106 (2002) 12737.
[25] J.L.G. Fierro, Stud. Surf. Sci. Catal. 130A (2000) 177.
[26] S. Velu, K. Suzuki, T. Osaki, Chem. Commun. (1999) 2341.
[27] U. Costantino, F. Marmottini, M. Nocchetti, R. Vivani, Eur. J. Inorg Chem. (1998) 1439.
[28] J. Agrell, H. Birgersson, M. Boutonnet, I. Meliàn-Cabrera, R.M. Navarro, J.L.G. Fierro, J. Catal. 219 (2003) 389.
[29] S. Velu, K. Suzuki, M.P. Kapoor, F. Ohashi, T. Osaki, Appl. Catal. A 213 (2001) 47.
[30] Y. Choi, H.G. Stenger, Appl. Catal. B 38 (2002) 259.
[31] R.O. Idem, N.N. Bakhshi, Chem. Eng. Sci. 51 (1996) 3697.
[32] S.J. Gregg, K.S.W. Sing, Adsorption, Surface Area and Porosity, Academic Press, London, 1982, p. 98.
[33] G.C. Bond, S.N. Namijo, J. Catal. 118 (1989) 507.
[34] A. Larson, R.B. Von Dreele, G.S.A.S., Generalized Structure Analysis System, Los Alamos National Laboratory, 1988.
[35] L. Latterini, F. Elisei, G.G. Aloisi, U. Costantino, M. Nocchetti, Phys. Chem. Chem. Phys. 4 (2002) 2792.
[36] S. Miyata, Clays Clay Miner. 31 (1983) 305.
[37] J.T. Kloprogge, R.L. Frost, in: V. Rives (Ed.), Layered Double Hydroxides: Present and Future, Nova Science, New York, 2001, p. 93.
[38] G. Busca, V. Lorenzelli, V. Sanchez Escribano, Chem. Mater. 4 (1992) 595.
[39] J. Preuhomme, P. Tarte, Spectrochim. Acta A 23 (1967) 2127.
[40] M.C.N.A. de Carvalho, F.B. Passos, M. Schmal, Appl. Catal. A 193 (2000) 265.
[41] K.I. Hadjiivanov, G.N. Vayssilov, Adv. Catal. 47 (2002) 307.
[42] G. Busca, J. Mol. Catal. 43 (1987) 225.
[43] J.M. Gallardo Amores, V. Sanchez Escribano, G. Busca, V. Lorenzelli, J. Mater. Chem. 4 (1994) 965.
[44] G. Busca, M.E. Pattuelli, F. Trifirò, A. Vaccari, in: A. Zecchina, G. Costa, C. Morterra (Eds.), Structure and Reactivity of Surfaces, Elsevier, Amsterdam, 1989, p. 239.
[45] K. Hadjiivanov, D. Klissurski, G. Ramis, G. Busca, Appl. Catal. B 7 (1996) 251.
[46] M. Trombetta, G. Ramis, G. Busca, B. Montanari, A. Vaccari, Langmuir 13 (1997) 4628.
[47] J.M. Gallardo Amores, V. Sanchez Escribano, G. Ramis, G. Busca, Appl. Catal. B 13 (1997) 45.
[48] M. Angeles Larrubia, G. Ramis, G. Busca, Appl. Catal. B 30 (2001) 101.
[49] G. Busca, R. Guidetti, V. Lorenzelli, J. Chem. Soc., Faraday. Trans. 86 (1990) 989.
[50] J. Agrell, K. Hasselbo, K. Jansson, S.G. Järas, M. Boutonnet, Appl. Catal. A 211 (2001) 239.
[51] Y. Liu, T. Hayakawa, K. Suzuki, S. Hamakawa, T. Tsunoda, T. Ishii, M. Kumagai, Appl. Catal. A 223 (2002) 137.